Toxicology Reports 2 (2015) 765–774

Contents lists available at ScienceDirect

Toxicology Reports

journal homepage: www.elsevier.com/locate/toxrep

Comparative study of the cytotoxic and genotoxic potentials of zinc oxide and titanium dioxide nanoparticles

Maryam Khan [a], Alim Husain Naqvi [b], Masood Ahmad [a,*]

[a] Department of Biochemistry, Faculty of Life Sciences, Aligarh Muslim University, Aligarh, UP 202002, India
[b] Centre of Excellence in Materials Science (Nanomaterials), Department of Applied Physics, Z.H. College of Engineering & Technology, Aligarh Muslim University, Aligarh, UP 202002, India

ARTICLE INFO

Article history:
Received 27 November 2014
Received in revised form 30 January 2015
Accepted 2 February 2015
Available online 19 February 2015

Keywords:
Zinc oxide nanoparticles
Titanium dioxide nanoparticles
Oxidative stress
Comet assay
Genotoxicity
DNA damage

ABSTRACT

Nanoparticles (NPs) of zinc oxide (ZnO) and titanium dioxide (TiO_2) are receiving increasing attention due to their widespread applications. The aim of this study was to evaluate the toxic effect of ZnO and TiO_2 NPs at different concentrations (50, 100, 250 and 500 ppm) and compare them with their respective salts using a battery of cytotoxicity, and genotoxicity parameters. To evaluate cytotoxicity, we have used human erythrocytes and for genotoxic studies human lymphocytes have been used as *in vitro* model species. Concentration dependent hemolytic activity to RBC's was obtained for both NPs. ZnO and TiO_2 NPs resulted in 65.2% and 52.5% hemolysis at 250 ppm respectively indicating that both are cytotoxic to human RBCs. Antioxidant enzymes assays were also carried out in their respective hemolysates. Both nanoparticles were found to generate reactive oxygen species (ROS) concomitant with depletion of glutathione and GST levels and increased SOD, CAT and lipid peroxidation in dose dependent manner. ZnO and TiO_2 NPs exerted roughly equal oxidative stress in terms of aforementioned stress markers. Genotoxic potential of both the NPs was investigated by *in vitro* alkaline comet assay. DNA damage induced by the NPs was concentration dependent and was significantly greater than their ionic forms at 250 and 500 ppm concentrations. Moreover, the nanoparticles of ZnO were significantly more genotoxic than those of TiO_2 at higher concentrations. The toxicity of these NPs is due to the generation of ROS thereby causing oxidative stress.

1. Introduction

Nanotechnology has gained a great deal of public interest due to increasing applications of nanomaterials (1–100 nm) in many areas of human endeavors such as industry, agriculture, business, medicine, public health *etc.* However, several studies conducted during the last few years indicate that nanoparticles (NPs) may interfere with cellular system by the interaction with proteins, DNA, lipids, membranes, organelles and biological fluids [1,2]. Because of their extremely small size and large surface area to volume ratio, they can easily cross the biological cells and membranes. Once inside the body, they can enter the bloodstream and hence reach different organs [3]. Although the mechanisms underlying the NPs toxicity are not yet clear, it has been suggested that oxidative stress and lipid peroxidation play an important role in DNA damage, cell membrane disruption and cell death [4–6].

According to U.S National Nanotechnology Initiative titanium dioxide nanoparticles (TiO_2 NPs) are one of the largest manufactured NPs in the world. They are used in variety of applications as paints, printing ink, rubber, paper,

* Corresponding author. Tel.: +91 897459786.
E-mail address: masoodamua@rediffmail.com (M. Ahmad).

http://dx.doi.org/10.1016/j.toxrep.2015.02.004

cosmetics, pharmaceuticals, sunscreens, car materials, implanted biomaterials and decomposing organic matters in waste water [7–9]. Zinc oxide nanoparticles (ZnO NPs) are widely used as nanosensors [10], UV-absorbers [11], and catalysts [12]. Zinc oxide (ZnO) nanoparticles are also employed in cosmetics and modern sunscreens, in coatings (UV protection) and electronic devices [13].

Due to the increasing common applications of ZnO and TiO_2 NPs in the market, it is essential to know the harmful effects caused by them on the health of individuals as well as the environment. The aim of the present study was to evaluate the toxic effects of ZnO and TiO_2 NPs in humans compared with their respective salts using a battery of cytotoxic, and genotoxic parameters so that their use is limited or else used in safe doses. Also, present study has demonstrated for the first time the *in vitro* generation of ROS by ZnO and TiO_2 NPs.

2. Materials and methods

Ethical statement

5 ml each of fresh human blood (self donor) was taken for both experiments *i.e.* hemolysis assay and comet assay. According to Indian Council for Medical Research, New Delhi, India, Chapter-II, page no.11–12, the ethical approval for this research was not deemed to be necessary. According to this guideline, proposals which present less than minimal risks are exempted from the ethical review process.

2.1. Chemicals and materials

5,5′-Dithiobis-(2-nitrobenzoic acid)-DTNB, ethylene diamine tetra acetic acid (EDTA), horse radish peroxidase (HRP), glutathione reduced, pyrogallol and heparin were obtained from Sisco Research Laboratories (SRL), India. Histopaque-1077, RPMI-1640 medium, low melting agarose and thiobarbituric acid (TBA) were purchased from Sigma Chemicals Co, USA. Trichloro acetic acid (TCA) was obtained from Qualigens Fine Chemicals, India while ethidium bromide (EtBr) from Hi Media, India Ltd. All other chemicals were of highest analytical grade available.

2.2. Preparation and characterization of nanoparticles

2.2.1. Preparation of ZnO nanoparticles

In a typical synthesis method, Zinc acetate [$(Zn(CH_3COO)_2{\cdot}2H_2O$] and citric acid (1:1 molar ratio) were dissolved in deionised water. The solution was stirred at 100 °C for 1 h (hour) till the formation of gel. The gel was burned at 200 °C and further annealed at 450 °C for 1 h to obtain the crystalline ZnO NPs [14].

2.2.2. Preparation of TiO_2 nanoparticles

TiO_2 NPs were synthesized by hydrolyzing titanium isopropoxide [$Ti\{OCH(CH_3)_2\}_4$] in a mixture of ethanol and water. The so obtained gel was dried at 80°C for 4 h. Finally, the white powder was calcined at 500 °C [15].

2.2.3. Characterization of nanoparticles

The ZnO and TiO_2 NPs prepared as above were characterized by X-ray diffraction (XRD) and transmission electron microscopy (TEM). The XRD pattern was obtained using X-ray diffractometer (Rigaku, Japan-Miniflex-II) using scan speed 4 steps/s and angle range (20–80°). The morphologies of both the NPs were examined by transmission electron microscopy (TEM-JEOL-2100F). Fourier transform infrared (FTIR) spectra of the samples were recorded using FTIR-Perkin Elmer instrument, USA (Spectrum-II, wave no. 4000–400).

2.3. Stock sample preparation

The ZnO and TiO_2 nanoparticles were suspended in distilled water and dispersed by ultrasonic vibrations (130 W, 20 kHz) for 20 min (minutes) for all experimental works.

2.4. Toxicological tests

2.4.1. Hemolysis

2.4.1.1. Isolation of erythrocytes from human blood. Heparinized fresh human blood was taken from young, healthy, non-smoking individual (self donor). It was centrifuged at 1500 rpm for 10 min at 4 °C in a clinical centrifuge and the plasma and buffy coat were removed by aspiration. The erythrocyte pellet was washed thrice with phosphate buffered saline (PBS) (0.01 M sodium phosphate buffer, 0.9% NaCl, pH 7.2) and resuspended in PBS to give a 5% hematocrit [16].

2.4.1.2. Treatment of erythrocytes with samples and preparation of lysates. Erythrocytes were incubated with different concentrations (50 ppm, 100 ppm, 250 ppm, 500 ppm) of both the NPs and their respective salts separately for 1 h at 37 °C. The samples were centrifuged at 2500 rpm for 10 min at 4 °C. The pellets so obtained were washed thrice with PBS and erythrocytes were lysed with 10 volumes of distilled water at 4 °C for 2 h. The hemolysates were centrifuged at 3000 rpm for 10 min at 4 °C and the supernatants were quickly frozen in aliquots and later used for biochemical estimations. Untreated erythrocytes were completely lysed with distilled water and used as reference.

2.4.1.3. Determination of total protein concentration. Total protein content in the hemolysates was estimated by Folin's reagent using bovine serum albumin as standard [17].

2.4.2. Assays of enzymatic and non-enzymatic antioxidants

2.4.2.1. Superoxide dismutase (SOD). SOD activity in the hemolysates was assayed by measuring its ability to inhibit the auto oxidation of pyrogallol according to the method of Marklund and Marklund [18]. To 50 μl of hemolysate, 2.85 ml of tris succinate buffer (0.05 M, pH 8.2) was added and the reaction was started by adding 100 μl of 8.0 mM pyrogallol. The change in absorbance was recorded at an interval of 30 s (seconds) for 3 min at 412 nm. A reference set containing 50 μl distilled water instead of hemolysate,

was also run simultaneously. The activity was reported in terms of U/mg protein.

2.4.2.2. Catalase (CAT). Catalase activity was measured essentially following the method of Aebi [19]. 3 ml reaction mixture contained 1.9 ml of 0.05 M potassium phosphate buffer (pH-7.4), 1 ml of 30 mM H_2O_2 and 100 μl of test sample's hemolysate and absorbance at 240 nm was recorded at an interval of 30 s for 3 min. Enzyme activity was calculated using the molar extinction coefficient of H_2O_2 as 436 mol l^{-1} cm^{-1} at 240 nm and reported in U/mg protein.

2.4.2.3. Lipid peroxidation (LPO). The extent of membrane lipid peroxidation was determined from malondialdehyde (MDA, an end product of LPO) content by the method of Beuge and Aust [20]. 1.0 ml of hemolysate was mixed with 2.0 ml of TBA–TCA–HCl reagent and the mixture was heated in boiling water bath for 15 min. After cooling to room temperature, the precipitate was removed by centrifugation at 4000 rpm for 10 min and absorbance of supernatant was recorded at 535 nm against a blank that contained all reagents except hemolysate. The MDA concentration was calculated using a molar extinction coefficient of 1.56×10^5 M^{-1} cm^{-1} and reported in nmole/mg protein.

2.4.2.4. Glutathione-S-transferase (GST). The activity of GST was assayed by the method as described by Habig et al. [21], using CDNB (1-chloro-2,4-dinitrobenzene) as substrate and measuring the amount of CDNB–GSH conjugate formed. Absorbance at 340 nm was recorded at an interval of 30 s for 3 min.

2.4.2.5. Glutathione (GSH) estimation. GSH levels were estimated by the method of Jollow et al. [22] using the classical DTNB reagent. 500 μl of 4% sulphosalicylic acid was added to 100 μl of hemolysate. It was left for incubation at 4 °C for 1 h. Then the mixture was centrifuged at 12,000 × *g* for 15 min at 4 °C and the supernatant was taken out. 0.4 ml of supernatant was mixed with 2.2 ml of potassium phosphate buffer (0.1 M, pH 7.4) and 0.4 ml DTNB (4 mg/ml). Yellow color developed by the reaction of GSH with DTNB was read at 412 nm. The concentration is reported in terms of nmole/mg protein.

2.4.3. Estimation of ROS generation in the test samples

2.4.3.1. Hydrogen peroxide. The amount of H_2O_2 in the test water sample was estimated by the horse radish peroxidase (HRPO) mediated oxidation of phenol red by H_2O_2 [23]. The reaction mixtures containing 2.8 ml phenol red (0.28 mM phenol red, 20 U ml^{-1} HRPO, 5.5 mM dextrose, 10 mM potassium phosphate buffer, pH 7.0), 100 μl of NaOH (1N) and different volumes of test samples (10 μl, 20 μl, 50 μl, 100 μl) were incubated at 37 °C for 10 min in dark. At the completion of incubation, the reaction mixture was centrifuged for 5 min at 2500 rpm at 4 °C. Absorbance was taken at 610 nm.

2.4.3.2. Hydroxyl radicals. The estimation of •OH radical was carried out by the method of Richmond et al. [24]. To different concentrations of test samples, 150 μl of Tris–HCl buffer (0.01 M, pH 7.5) and 300 μl of calf thymus DNA (3.0 mM) were added, and the mixture was incubated for 1 h at 37 °C. This is followed by the addition of 1.2 ml of 28% TCA, to stop the reaction. After that 1.2 ml of 1% TBA was added and test tubes were boiled for 15 min. After cooling the test tubes to room temperature, absorbance was recorded at 532 nm.

2.4.3.3. Super-oxide radical. The estimation of $O_2^{\bullet -}$ was done by NBT–$O_2^{\bullet -}$ determination method of Nakayama et al. [25]. The reaction mixture contained 300 μl of sodium phosphate buffer (100 mM, pH-8), 100 μl of NBT (1 mM), 300 μl of triton-X-100 (0.6%), 2.2 ml of D.W., and different volumes of test samples (10 μl, 20 μl, 50 μl, 100 μl). Absorbance was taken at 560 nm.

2.4.4. Comet assay (single cell gel electrophoresis)

2.4.4.1. Isolation of lymphocytes. Heparinized blood sample was obtained from a single healthy volunteer (self donor) and diluted suitably in saline in 1:1 ratio. 1/3 of the total volume, histopaque 1077 (Sigma, USA; density – 1.077) was taken in a centrifuge tube and the diluted blood was added along the sides of the tube over the histopaque. The blood was centrifuged at 2400 rpm for 20 min. The cloudy layer seen at the junction was pipetted out very carefully and the lymphocytes were diluted with saline in 1:1 ratio. 100λ of diluted lymphocytes were taken in each microfuge tube.

2.4.4.2. Experimental procedure. Comet assay was performed under alkaline conditions according to the procedure of Singh et al. [26] with slight modifications. Fully frosted microscopic slides pre-coated with 1.0% normal melting agarose. Diluted lymphocytes were then mixed properly with equal volume of 2.0% low melting agarose and half of the mixture was pipetted over the first layer. The slides were covered immediately by cover slips and placed on ice for 15 min to solidify. Immediately after removing the cover slips, within 20 min cells were treated with increasing concentrations of samples (0–500 ppm) for 1 h at 4 °C. Lysis was done in cold lysis solution containing 2.5 M NaCl, 100 mM EDTA, 10 mM Tris (pH 10) and 1% Triton X-100 (added just prior to use) for 1 h at 4 °C followed by unwinding of DNA for 30 min in alkaline electrophoretic solution containing 300 mM NaOH, 1 mM EDTA, pH 13 (at 4 °C, 300 mA current). After electrophoresis, DNA was neutralized in neutralizing solution (0.4 M Tris, pH 7.5). The slides were stained with 75 μl ethidium bromide (EtBr, 20 μg/ml), washed with distilled water, covered with cover slips and placed in a humidified chamber.

2.4.4.3. Visualization of slides and scoring. Slides were visualized using an image analysis system (Komet 5.5; Kinetic Imaging, Liverpool, UK) attached to an Olympus (CX41) fluorescent microscope (Olympus Optical Co., Tokyo, Japan) and a COHU 4910-integrated CC camera (equipped with 510–560 nm excitation and 590 nm barrier filters) (COHU, San Diego, USA). Images from 50 cells (25 from each replicate slide) were analyzed. Tail length (migration of DNA from the nucleus in μm) was chosen as the parameter to assess DNA damage.

2.5. Statistical evaluation

Data was expressed as mean ± S.D. of three independent experiments and statistical analysis was performed by one way ANOVA test. Differences among control and treated groups were determined using student's *t*-test. *p* values of ≤0.05 were considered statistically significant. All comparisons were made with ionic forms (serving as positive control) and untreated cells (serving as negative control).

3. Results

3.1. Nanoparticles characterization

3.1.1. X-ray diffraction

Fig. 1(a) shows X-ray diffraction pattern of zinc oxide nanoparticles. Highly intense peaks observed in the XRD pattern indicated that ZnO NPs were well crystalline. The peaks were obtained in the samples at $2\theta = 31.2^\circ$, 33.9°, 35.5°, 46.9°, 56.0°, 62.0°, 67.0°, hence no diffraction peaks of other impurities were detected, which confirmed that the prepared sample was pure ZnO NPs. Similar results were also reported by others [27–30]. The crystal size of the ZnO NPs calculated from the XRD spectra was found to be 17.1 nm.

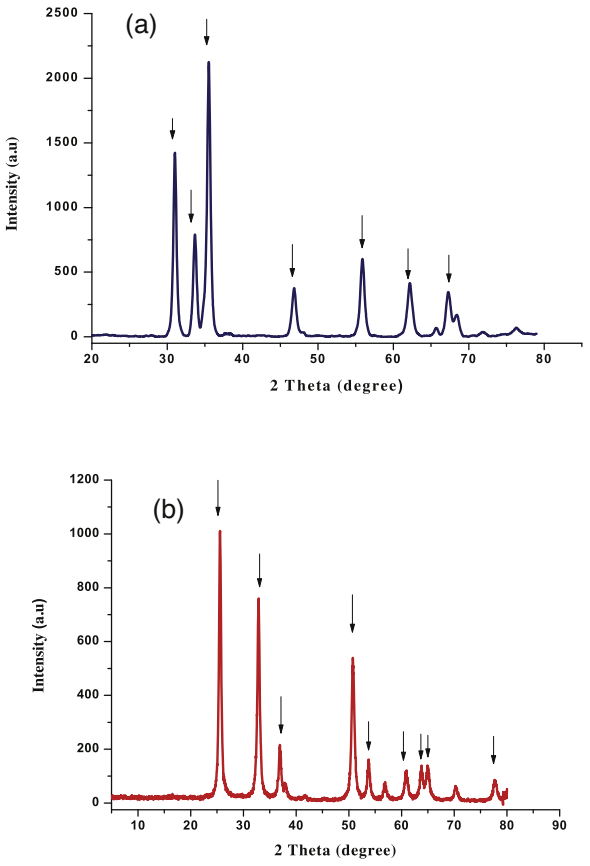

Fig. 1. (a) XRD pattern of ZnO nanoparticles. (b) XRD pattern of TiO_2 nanoparticles.

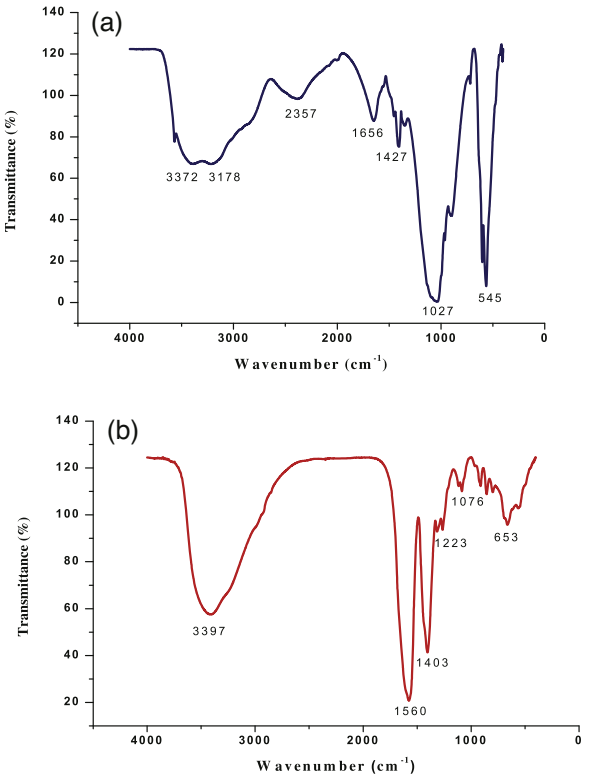

Fig. 2. (a) FTIR spectra of ZnO nanoparticles. (b) FTIR spectra of TiO_2 nanoparticles.

Fig. 1(b) shows the X-ray diffraction (XRD) pattern of TiO_2 NPs. Peaks at 25.8°, 32.9°, 37.0°, 50.7°, 53.0°, 61.0°, 63.0°, 69.0°, 77.1° were observed which confirms the formation of mixed phase of TiO_2 NPs (anatase and rutile). Similar results were also obtained by Chaudhary et al. [31], Ba-Abbad et al. [32] and Hema et al. [33]. The appearance of sharp diffraction patterns indicates the small size, high purity and crystallinity of the synthesized sample [34]. Diffraction pattern corresponding to impurities were found to be absent. In the present study, the size of the TiO_2 NPs crystals calculated from the XRD spectra was found to be 17.8 nm.

3.1.2. Fourier transmission infrared spectroscopy

Fig. 2(a) shows FTIR spectra of the ZnO NPs. FTIR studies were carried out to ascertain the purity and nature of these nanoparticles. Metal oxides generally give absorption bands in fingerprint region *i.e.* below 1000 cm^{-1} arising from inter-atomic vibrations. The peaks observed at 3372 and 3178 cm^{-1} are due to O—H stretching [35]. Peaks at 1656 cm^{-1} and 1427 cm^{-1} correspond to C=C stretch and C—C stretching respectively. The peaks at 1027 and 545 cm^{-1} are the characteristic absorption peaks of Zn–O bond and also authenticates the presence of ZnO [35,36].

FTIR spectrum of the TiO_2 NPs is shown in Fig. 2(b). Peaks at 3397 cm^{-1} correspond to stretching vibrations of O—H bond [33]. Peaks observed at 1560 and 1403 are attributed to C—C stretching. Sharp peaks at 1223 and 1056 cm^{-1} are

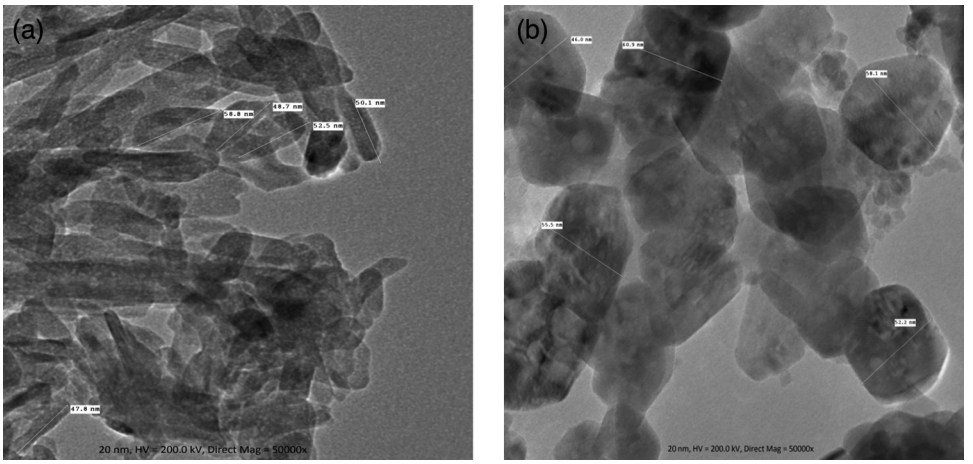

Fig. 3. (a) TEM image of ZnO nanoparticles. (b) TEM image of TiO_2 nanoparticles.

due to C—O stretching [33]. Peaks observed at 846 cm^{-1} and 653 cm^{-1} indicated Ti—O vibrations [32].

3.1.3. Transmission electron microscopy

Fig. 3(a) shows the TEM image of ZnO NPs. Rod shaped ZnO NPs were observed in TEM images with average size in the range of 47.8–52.5 nm. The particle size and shape of TiO_2 nanoparticles were determined by TEM and shown in Fig. 3(b). The TEM image shows that the TiO_2 NPs are roughly spherical with an average size in the range of 46.0–60.9 nm.

3.2. Toxicity tests

3.2.1. Hemolysis

Fig. 4 shows the plot of percent hemolysis with increasing concentrations of both NPs and their respective salts in the range of 50–500 ppm. ZnO and TiO_2 NPs showed 65.2% and 52.5% hemolysis respectively at 250 ppm (Fig. 4). Statistical analysis was performed between the individual NPs and their respective ionic forms. Based on ANOVA test, we found statistically insignificant difference between the cytotoxicity of NPs and their respective ions.

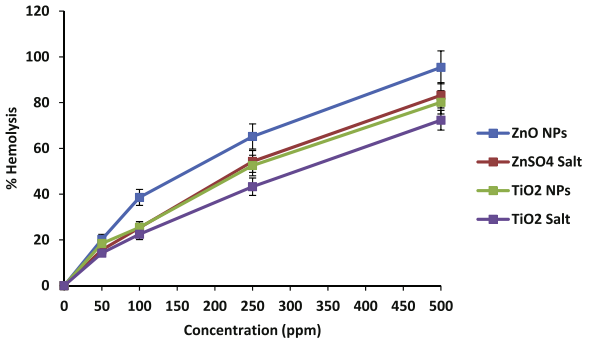

Fig. 4. Increasing rates of hemolysis in human erythrocytes upon incubation with increasing concentrations of ZnO and TiO_2 nanoparticles and their ionic counterparts. Data represent mean ± S.D. of three individual experiments, p-value ≤0.05.

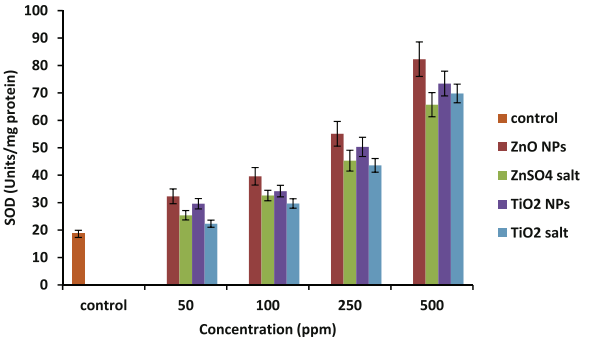

Fig. 5. Increasing activity of SOD in hemolysates prepared before and after treatment with increasing concentrations of ZnO and TiO_2 nanoparticles along with their respective salts. Data represent mean ± S.D. of three individual experiments, p-value ≤0.05.

3.2.2. Oxidative stress markers

Figs. 5 and 6 present the activity profiles of superoxide dismutase (SOD) and catalase (CAT) respectively in the hemolysates upon treatment with nanoparticles as well as with their respective ionic forms. At 500 ppm, ZnO NPs showed 77% more increase with respect to untreated

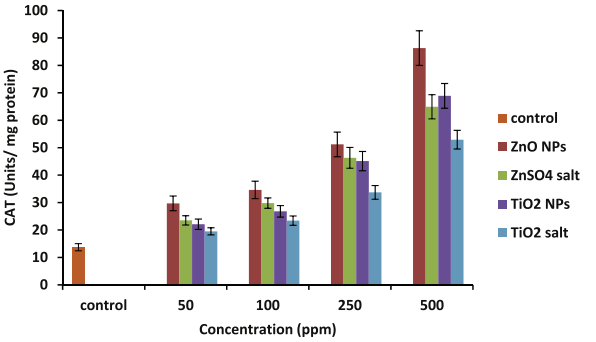

Fig. 6. Activity profile of CAT in hemolysates prepared before and after incubation with increasing concentrations of ZnO and TiO_2 nanoparticles and their respective ions. CAT activity was increased with respect to control, significant increase at 250 and 500 ppm. All values represent mean ± S.D. of three individual experiments (n = 3), p-value ≤0.05.

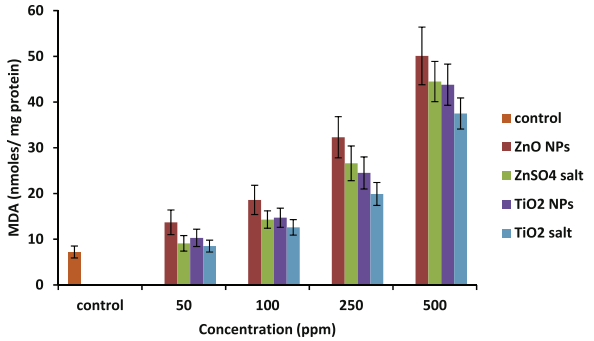

Fig. 7. Increasing MDA levels in hemolysates prepared before and after treatment with increasing concentrations of ZnO and TiO_2 nanoparticles and their ionic forms. Data represent mean ± S.D. ($n = 3$), p-value ≤0.05.

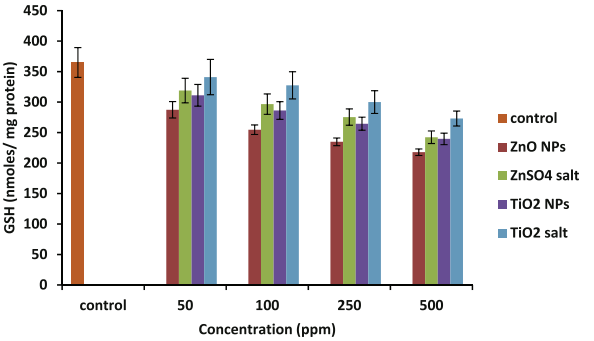

Fig. 9. Levels of reduced glutathione (GSH) in hemolysates prepared before and after exposure increasing concentrations of ZnO and TiO_2 nanoparticles as well as their ionic counterparts. Data represent mean ± S.D. ($n = 3$), p-value ≤0.05.

control (p-value ≤ 0.05), and TiO_2 NPs showed an increase upto 74% in SOD activity. A rise of around 84% in CAT level was observed at 500 ppm concentration of ZnO nanoparticles. Exposure with the same concentration of TiO_2 NPs showed an increase by 80% in CAT activity with respect to untreated control.

The effects of increasing concentrations of ZnO and TiO_2 NPs along with their ionic forms on the extent of LPO, measured in terms of MDA level are shown in Fig. 7. A significant elevation in malondialdehyde (MDA) levels of nanoparticle treated erythrocytes was recorded. At 500 ppm, ZnO NPs showed 85% increase in activity, and TiO_2 nanoparticles showed around 83% rise compared with the negative control (p-value ≤ 0.05).

Fig. 8 gives the trend of GST activity in hemolysates exposed to different concentrations of test samples. There was a decline in GST activity with increasing concentrations of the test samples which were statistically significant at 250 ppm and 500 ppm concentrations only. It was decreased up to 79% compared with control in case of ZnO NPs and 70% in case of TiO_2 NPs.

The pattern of change in activity profile of GSH in the hemolysates after treatment with different concentrations of ZnO and TiO_2 NPs is depicted in Fig. 9. The increasing concentrations of both the NPs had only diminutive effect on GSH level. Both ZnO NPs and TiO_2 NPs induced a dose-dependent and roughly equal decline in GSH concentration.

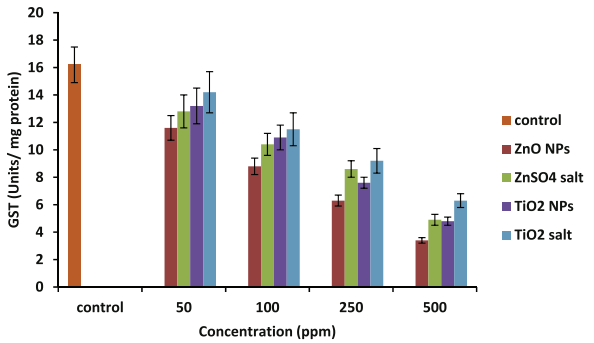

Fig. 8. Declining activity of GST in hemolysates prepared before and after incubation with increasing concentrations of ZnO and TiO_2 nanoparticles and their respective ions. Data represent mean ± S.D. ($n = 3$), p-value ≤0.05.

ZnO NPs at 500 ppm concentration, the levels decreased by 33% and TiO_2 NPs at same concentration decreased the GSH level with respect to control by 30%.

3.2.3. *In vitro ROS generation*

Fig. 10 shows the profiles of *in vitro* ROS generation profiles by both ZnO and TiO_2 NPs and their ionic forms. Both nanoparticles were found to generate all the three ROS namely superoxide radicals, hydroxyl radicals and hydrogen peroxide. However, ZnO nanoparticles showed a higher generation of ROS compared with TiO_2 NPs. Interestingly, the ionic forms of both NPs here showed a significantly lesser degree of ROS generation (p-value ≤ 0.05).

3.2.4. *Comet assay*

The tail lengths (parameter of DNA damage) are plotted with increasing concentrations of ZnO and TiO_2 NPs as well as their ionic forms in Fig. 11. The figures depict a dose-dependent DNA damage in terms of tail length in all the four cases. At 500 ppm, the ZnO NPs showed 13% more DNA damage to human lymphocyte indicating thereby a higher genotoxic potential of ZnO NPs compared to TiO_2 NPs though not a significant one.

4. Discussion

Owing to the growing applications of metal oxide NPs in various household products and industry, their release into the environment may pose serious threats to ecological systems and human health [37–40]. Some investigators have worked on the toxic effects of nanoparticles on various organs and systems [41–43]. Nevertheless, there is a general lack of information concerning the effects of manufactured nanomaterials on humans, especially the studies on the toxic effects of nanoparticles are in preliminary stages and nothing is known about their mode of action, target sites and effectiveness [44]. Since most of the future applications of therapeutic nanoparticles are based on intravenous or oral administration, their interaction with human blood components is of extreme importance. We have used human erythrocytes as well as lymphocytes in our *in vitro* studies to assess the adverse effects caused by ZnO and TiO_2 NPs.

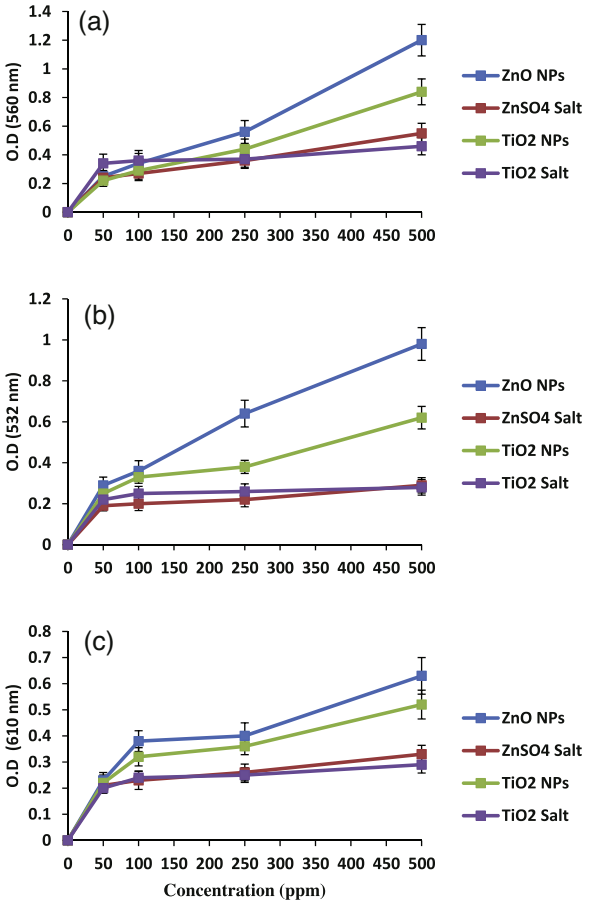

Fig. 10. Typical patterns of *in vitro* generation of different ROS *i.e.* (a) superoxide radicals (b) hydroxyl radicals, and (c) hydrogen peroxide by ZnO and TiO_2 nanoparticles and their respective ions. In all the three graphs, the nanoforms of ZnO and TiO_2 exhibited a greater release of ROS as compared to their respective ionic counterparts. Data represent mean ± S.D. ($n = 3$), p-value ≤0.05.

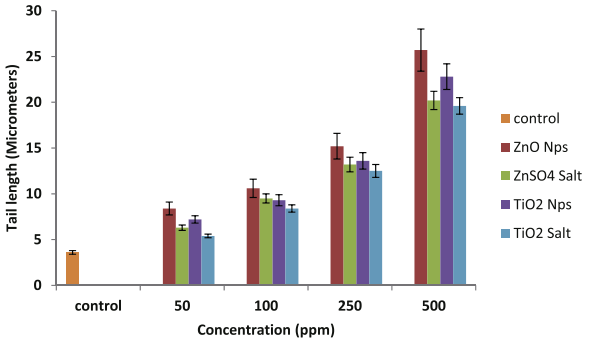

Fig. 11. Increasing DNA damage in human lymphocytes measured in terms of tail length after exposure to different concentrations of ZnO and TiO_2 nanoparticles and their respective ions. Significant increase in tail length was observed at 100, 250 and 500 ppm with respect to control. ZnO NPs showed significant DNA damage at 500 ppm as compared to TiO_2 NPs Data represent mean ± S.D. ($n = 3$), p-value ≤0.05.

Present study deals with the comparative analysis of the cytotoxicity and genotoxicity of the ZnO and TiO_2 NPs along with their respective ionic forms. To assess the toxicity of NPs at the cellular level, hemolysis assay was performed. The rationale for this assay was to evaluate the mechanical damage by NPs vis-à-vis respective ionic forms on the RBC'S membrane. Moreover, human blood is the ultimate target of these NPs in the human body. A concentration dependent hemolytic activity was recorded for both the NPs as well as their ionic forms. ZnO NPs were found to show a significantly higher hemolytic activity as compared to TiO_2 NPs at all experimental treatments. However, both the nanoforms did not show any significant difference in cytotoxicity when compared to their respective ions. Abott et al. [45] also reported a higher cytotoxicity of ZnO NPs on Caco-2 and SW480 human intestinal epithelial cells as compared to TiO_2 NPs. Dose dependent cytotoxicity of TiO_2 NPs was also recorded by Li et al. [46].

Oxidative stress is said to be the main mechanism of nanoparticle toxicity [4–6]. In the present study, both ZnO and TiO_2 NPs seem to have triggered oxidative stress in human erythrocytes which is evident from the typical changes in SOD, CAT and GST as well as in the levels of glutathione (GSH) and MDA (Figs. 5–9).

In our study, both SOD and CAT levels showed a dose dependent increase in their activity. There was a significant rise in SOD and CAT levels with respect to control (p-value ≤ 0.05) by both the NPs as well as their ionic forms at higher concentrations of 250 ppm and 500 ppm only (Figs. 5 and 6). SOD activity profile suggests that ionic forms of ZnO were found to be significantly less toxic than its nanoform at 250 and 500 ppm concentrations while in case of TiO_2, no significant difference was found between the nano and the ionic forms. Looking at the CAT activity profile, both the NPs have shown a significantly higher response (increase in CAT activity) compared to ionic forms at higher doses. Rise in SOD and CAT activities was also recorded in cells of *Oreochromis mossambicus* and mouse liver exposed to ZnO NPs respectively [47,48] which are consistent with our results.

LPO can be defined as the oxidative deterioration of cell membrane lipids and has been used extensively as a marker of oxidative stress [49]. LPO is estimated by measuring the content of MDA. The over-accumulation of MDA can damage cells and trigger apoptosis [50]. Our study showed a continuous rise in MDA activity up to the maximum experimental concentration. Moreover, both the nanoforms displayed a higher response toward MDA activity compared with their ionic forms although the change is not significant (p-value ≤ 0.05; Fig. 7). According to the graph, there was an insignificant difference between ZnO and TiO_2 NPs in response to MDA levels. Meena et al. [51] also reported an increase in MDA levels in HEK cells exposed to TiO_2 nanoparticles.

There was a gradual decrease in the GST activity as a result of increasing concentrations of both the test nanoparticles and their ionic forms (Fig. 8). The decrease was significant only at 250 ppm and 500 ppm concentrations for all the samples. Also, when both the NPs were compared with their ionic counterparts, they were found to significantly differ in their response toward GST

activity at higher concentrations *i.e.* at 250 and 500 ppm only. Both exhibited roughly equal degree of change in GST activity at 50 and 100 ppm concentrations. Decrease in GST levels by the exposure of ZnO NPs and Zn^{2+} ions to fish cells was reported by Fernandez et al. [52]. Our findings are consistent with their results in terms of higher cytotoxicity of ZnO NPs than those of Zn^{2+} ions.

Another marker of response to oxidative stress that we monitored in the present study was the change in the intracellular GSH levels, which has been often shown to be involved in cellular responses to toxins and xenobiotics [53]. GSH levels are supposed to be suppressed under severe oxidative stress due to loss of compensatory responses and oxidative conversion of GSH to its oxidized form [54]. Our results indicated a slight decline in GSH levels in the hemolysates treated with all the four samples with respect to untreated control but not statistically significant one among the two NPs and their ionic forms (Fig. 9). GSH levels have been reported to be decreased significantly after oral administration of ZnO NPs in lung tissue [55]. In the present study, the ZnO NPs showed an insignificant difference in GSH activity compared to their ionic forms. However, the TiO_2 NPs exhibited significantly greater decline in the GSH activity in comparison to their ionic forms only at higher concentrations.

These nanoparticles have been found to generate reactive oxygen species in living system as reported by recent studies [56–58]. However, our study is the first to demonstrate the *in vitro* generation of ROS by nanoparticles in a dose dependent manner (Fig. 10). ZnO nanoparticles showed a higher generation of all the three species *i.e.* superoxide radicals, hydroxyl radicals and hydrogen peroxide compared to TiO_2 NPs. Moreover, both the nanoforms showed a significantly greater ROS generation compared to the ionic forms of ZnO and TiO_2 (p-value ≤ 0.05).

Genotoxicity of ZnO and TiO_2 nanoparticles was also evaluated by *in vitro* comet assay in human lymphocytes. As evident from the figure (Fig. 11), ZnO NPs induced a higher DNA damage to human lymphocyte compared with TiO_2 NPs. Furthermore, at 500 ppm concentration, both ZnO and TiO_2 NPs have shown a significant increase in tail length as compared to their ionic forms with p-value ≤ 0.05. These results are in conformity with our results of hemolysis, antioxidant enzymes and ROS generation. A recent report by Demir et al. [59] also affirms the genotoxic potential of zinc oxide (ZnO, $\leq$35 and 50 nm) and titanium dioxide (TiO_2, 21 and 50 nm) nanoparticles in the nuclei of *Allium cepa* root meristem cells by using a modified alkaline comet assay. The authors had taken three different concentrations *i.e.* 10, 100 and 1000 μg/ml and their results indicated that ZnO showed genotoxicity at 100 and 1000 μg/ml concentrations while TiO_2 NPs exhibited DNA damage only at the highest concentration inferring that ZnO is more genotoxic compared to TiO_2 NPs. Musarrat et al. [60] had also reported dose dependent genotoxic effect of ZnO NPs in human lymphocytes by the use of alkaline comet assay. Their results showed an increase in tail length with increasing concentrations of ZnO NPs again indicating the toxic nature of ZnO NPs.

5. Conclusions

Although we have demonstrated the *in vitro* generation of ROS directly for the first time, the genotoxicity and cytotoxicity assay conducted on the ZnO and TiO_2 NPs were also suggesting the role of ROS in the test NPs mediated toxicity. This study is also the first to examine the comparative hemolytic activities of ZnO and TiO_2 NPs. ROS generation has also shown to induce hemolysis [61]. Therefore, we can affirm that ROS generation is the main mechanism to cause various types of toxicities by ZnO and TiO_2 nanoparticles.

Present results clearly suggest that both zinc oxide and titanium dioxide in nanoform are significantly cytotoxic as well as genotoxic at all concentrations with respect to untreated sample or control. However, comparing with the ionic forms, no significant difference was obtained. Moreover, the ZnO NPs were found to exhibit significantly greater toxicity at higher concentrations compared to those of TiO_2 in terms of cytotoxic and genotoxic effects. The above mentioned toxicological tests and the resulting database would provide information for material safety data sheets for NPs as well as a basis for their risk assessments and risk management. However, the actual and precise conclusion can only be drawn after more intensive experimental works are carried out by using the whole animal or the cell lines for such studies.

Conflict of interest

The authors declare that there is no conflict of interest.

Transparency document

The Transparency document associated with this article can be found in the online version.

Acknowledgements and declarations

MK gratefully acknowledges the financial assistance in terms of JRF by UGC-MANF, New Delhi. The nanoparticles were prepared and characterized in the lab of AHN.

References

[1] Y. Roiter, M. Ornatska, A.R. Rammohan, J. Balakrishnan, D.R. Heine, S. Minko, Interaction of nanoparticles with lipid membrane, Nano Lett. 8 (2008) 941–944.
[2] L. Shang, L. Yang, J. Seiter, M. Heinle, G. Brenner-Weiss, D. Gerthsen, G.U. Nienhaus, Nanoparticles interacting with proteins and cells: a systematic study of protein surface charge effects, Adv. Mater. Interfaces 1 (2014) 1300079, http://dx.doi.org/10.1002/admi.201300079.
[3] V. Vishwakarma, S. Samal, N. Manoharan, Safety and risk associated with nanoparticles—a review, Min. Mater. Char. Eng. 9 (2010) 455–459.
[4] T. Xia, M. Kovochich, J. Brant, M. Hotze, J. Sempf, Comparison of the abilities of ambient and manufactured nanoparticles to induce cellular toxicity according to an oxidative stress paradigm, Nano Lett. 6 (2006) 1794–1807.
[5] Y. Hsin, C. Chen, S. Huang, T. Shih, P. Lai, The apoptotic effect of nanosilver is mediated by a ROS- and JNK-dependent mechanism involving the mitochondrial pathway in NIH3T3 cells, Toxicol. Lett. 179 (2008) 130–139.
[6] J.F. Reeves, S.J. Davies, N.J.F. Dodd, A.J. Jha, Hydroxyl radicals (*OH) are associated with titanium dioxide (TiO_2) nanoparticle-induced cytotoxicity and oxidative DNA damage in fish cells, Mutat. Res. 640 (2008) 113–122.

[7] T. Kaida, K. Kobayashi, M. Adachi, F. Suzuki, Optical characteristics of titanium oxide interference film and the film laminated with oxides and their applications for cosmetics, J. Cosmet. Sci. 55 (2004) 219–220.
[8] R. Wolf, H. Matz, E. Orion, J. Lipozencic, Sunscreens – the ultimate cosmetic, Acta Dermatovenerol. Croat. 11 (2003) 158–162.
[9] Y.T. Sul, Electrochemical growth behavior, surface properties, and enhanced in vivo bone response of TiO_2 nanotubes on microstructured surfaces of blasted, screw-shaped titanium implants, Int. J. Nanomed. 5 (2010) 87–100.
[10] K.J. Cash, H.A. Clark, Nanosensors and nanomaterials for monitoring glucose in diabetes, Trends Mol. Med. 16 (2010) 584–593.
[11] A. Becheri, M. Durr, P. Lo Nostro, P. Baglioni, Synthesis and characterization of zinc oxide nanoparticles: application to textiles as UV-absorbers, J. Nanoparticle Res. 10 (2008) 679–689.
[12] J. Strunk, K. Kahler, X. Xia, M. Muhler, The surface chemistry of ZnO nanoparticles applied as heterogeneous catalysts in methanol synthesis, Surf. Sci. 603 (2009) 1776–1783.
[13] A. Hernandezbattez, R. Gonzalez, J. Viesca, J. Fernandez, J. Diazfernandez, et al., CuO, ZrO_2 and ZnO nanoparticles as antiwear additive in oil lubricants, Wear 265 (2008) 422.
[14] S.A. Ansari, A. Nisar, B. Fatma, W. Khan, A.H. Naqvi, Investigation on structural, optical and dielectric properties of Co doped ZnO nanoparticles synthesized by gel-combustion route, Mater. Sci. Eng. 175 (2012) 428–435.
[15] M.S. Takriff, M.M. Ba-abbad, A.A.H. Kadhum, A.B. Mohamad, K. Sopian, Solar photocatalytic degradation of 2,4-dichlorophcnol by TiO_2 nanoparticle prepared by sol–gel method, Adv. Mater. Res. 6 (2008) 233–235.
[16] A.K. Gupta, M. Ahmad, Assessment of cytotoxic and genotoxic potential of refinery waste effluent using plant, animal and bacterial systems, J. Hazard. Mater. 201–202 (2012) 92–99.
[17] O.H. Lowry, N.J. Rosebrough, A.L. Fare, R.J. Randall, Protein measurement with the folin phenol reagent, Biol. Chem. 193 (1951) 265–275.
[18] S. Marklund, G. Marklund, Involvement of the superoxide anion radical in the autoxidation of pyrogallol and a convenient assay for superoxide dismutase, Eur. J. Biochem. 47 (1974) 469–474.
[19] H. Aebi, Catalase in vitro, Methods Enzymol. 105 (1984) 121–126.
[20] J.A. Beuge, S.D. Aust, Microsomal lipid peroxidation methods, Enzymol. 52 (1978) 302–310.
[21] W.H. Habig, M.J. Pabst, W.B. Jakoby, Glutathione S-transferases. The first enzymatic step in mercapturic acid formation, J. Biol. Chem. 249 (1974) 7130–7139.
[22] D.J. Jollow, J.R. Mitchel, N. Zampaglione, J.R. Gillete, Bromobenzene-induced liver necrosis, protective role of glutathione and evidence for 3,4-bromobenzene oxide as the hepatotoxic metabolite, J. Pharmacol. 11 (1974) 151–169.
[23] E. Pick, Y. Keisari, A simple colorimetric method for the measurement of hydrogen peroxide produced by cells in culture, J. Immunol. Methods 38 (1980) 161–170.
[24] R. Richmond, B. Halliwell, J. Chauhan, A. Darbre, Superoxide-dependent formation of hydroxyl radicals: detection of hydroxyl radicals by the hydroxylation of aromatic compounds, Anal. Biochem. 118 (1981) 328–335.
[25] T. Nakayama, T. Kimura, T. Kodama, C. Nagata, Generation of hydrogen peroxide and superoxide anion radical from active metabolites of naphthylamines and aminoazo dyes: it's possible role in carcinogenesis, Carcinogenesis 4 (1983) 765–769.
[26] N.P. Singh, M.T. McCoy, R.R. Tice, E.L. Schneider, A simple technique for quantitation of low levels of DNA damage in individual cells, Exp. Cell Biol. 175 (1988) 184–191.
[27] U. Ozgur, Y.I. Alivov, C. Liu, A. Teke, M. Reshchikov, et al., A comprehensive review of ZnO materials and devices, J. Appl. Phys. 62 (2005) 487–492.
[28] C. Jagadish, S.J. Pearton, Zinc Oxide Bulk, thin Films and Nanostructure, vol. 12, Elsevier, 2006, pp. 267–283.
[29] C. Klingshirn, ZnO: material, physics and applications, Chem. Phys. Chem. 86 (2007) 782.
[30] S. Baruah, J. Dutta, Hydrothermal growth of ZnO nanostructures, Sci. Technol. Adv. Mater. 10 (2009) 013001.
[31] V. Chaudhary, A.K. Srivastava, J. Kumar, On the sol–gel synthesis and characterization of titanium oxide nanoparticles, Mater. Res. Soc. Symp. Proc. Mater. Res. Soc. 1352 (2011), http://dx.doi.org/10.1557/opl.2011.759.
[32] M.M. Ba-Abbad, A.A.H. Kadhum, A.B. Mohamad, A.S. Takriff, K. Sopian, Synthesis and catalytic activity of TiO_2 nanoparticles for photochemical oxidation of concentrated chlorophenols under direct solar radiation, Int. J. Electrochem. Sci. 7 (2012) 4871–4888.
[33] M. Hema, A.Y. Arasi, P. Tamilsevi, R. Ranbarasan, Titania nanoparticles synthesized by sol–gel technique, Chem. Sci. Trans. 2 (2013) 239–245.
[34] W. Yang, F. Gao, G. Wei, L. An, Ostwald ripening growth of silicon nitride nanoplates, Cryst. Growth Des. 10 (2010) 29–31.
[35] H. Kumar, R. Rani, Structural and optical characterization of ZnO nanoparticles synthesized by microemulsion route, Int. Lett. Chem. Phys. Astron. 14 (2013) 26–36.
[36] K. Nejati, Z. Rezvani, R. Pakizevand, Synthesis of ZnO nanoparticles and investigation of the ionic template effect on their size and shape, Int. Nano Lett. 1 (2011) 75–81.
[37] M.C. Roco, Environmentally responsible development of nanotechnology, Environ. Sci. Technol. 39 (2005) 106–112.
[38] S.J. Klaine, P.J. Alvarez, G.E. Batley, T.F. Fernandes, R.D. Handy, et al., Nanomaterials in the environment: behavior, fate, bioavailability, and effects, Environ. Toxicol. Chem. 27 (2008) 1825–1851.
[39] W. Lin, Y. Huang, X.D. Zhou, Y. Ma, In vitro toxicity of silica nanoparticles in human lung cancer cells, Toxicol. Appl. Pharmacol. 217 (2006) 252–259.
[40] C. Marambio-Jones, E.M.V. Hoek, A review of the antibacterial effects of silver nanomaterials and potential implications for human health and the environment, J. Nanoparticle Res. 12 (2010) 1531–1551.
[41] J.C.K. Lai, M.B. Lai, S. Jandhyam, et al., Exposure to titanium dioxide and other metallic oxide nanoparticles induces cytotoxicity on human neural cells and fibroblasts, Int. J. Nanomed. 3 (2008) 533–545.
[42] A.R. Murray, E. Kisin, S.S. Leonard, S.H. Young, C. Kommimeni, V. Ekagan, et al., In vivo immunological toxicity in mice of carbon nanotubes with impurities, Toxicology 257 (2009) 161–167.
[43] S. Sharma, S.F. Ali, S.M. Hussain, S.S. Schlager, A. Sharma, Influence of engineered nanoparticles from metals on the blood brain barrier permeability, cerebral blood flow, brain edema and neurotoxicity- an experimental study in the rat and mice using behavioral and morphological approaches, Nanosci. Nanotechnol. 9 (2009) 5055–5072.
[44] C. Buzea, I. Ivan, P. Blandino, K. Robbie, Nanomaterials and nanoparticles: sources and toxicity, Biointerphases 2 (2007) 17–172.
[45] T.E. Abbott Chalew, K.J. Schwab, Toxicity of commercially available engineered nanoparticles to Caco-2 and SW480 human intestinal epithelial cells, Cell Biol. Toxicol. 29 (2013) 101–116.
[46] S.Q. Li, R.R. Zhu, H. Zhu, M. Xue, X.Y. Sun, S.D. Yao, et al., Nanotoxicity of TiO_2 nanoparticles to erythrocyte in vitro, Food Chem. Toxicol. 46 (2008) 3626–3631.
[47] P. Subramanian, G. Bupesh, Screening of enzyme biomarker for nanotoxicity of zinc oxide in *Oreochromis mossambicus*, AIP Conf. Proc. 1326 (2011) 80.
[48] S. Syama, S.C. Reshma, P.J. Sreekanth, H.K. Varma, P.V. Mohanan, Effect of zinc oxide nanoparticles on cellular oxidative stress and antioxidant defense mechanisms in mouse liver, Toxicol. Environ. Chem. 95 (2013) 495–503.
[49] I. Sayeed, S. Parvez, S. Pandey, B. Bin-Hafeez, R. Haque, S. Raisuddin, Oxidative stress biomarkers of exposure to deltamethrin in freshwater fish, *Channa punctatus* Bloch, J. Ecotoxicol. Environ. Safety 56 (2003) 295–301.
[50] X.H. Kong, G.Z. Wang, S.J. Li, Antioxidation and ATPase activity in the gill of mud crab *Scylla serrata* under cold stress, Chin. J. Oceanol. Limnol. 25 (2007) 221–226.
[51] R. Meena, R. Pal, S.N. Pradhan, M. Rani, R. Paulraj, Comparative study of TiO_2 and $TiSiO_4$ nanoparticles induced oxidative stress and apoptosis of HEK-293 cells, Adv. Mater. Lett. 3 (2012) 459–465.
[52] D. Fernandez, C. Garcia-Gomez, M. Babin, In vitro evaluation of cellular responses induced by ZnO nanoparticles, zinc ions and bulk ZnO in fish cells, Sci. Total Environ. 452–453 (2013) 262–274.
[53] B. Zegura, T.T. Lah, M. Filipic, Alteration of intracellular GSH levels and its role in microcystin-LR-induced DNA damage in human hepatome HepG2 cells, Mutat. Res. 611 (2006) 25–33.
[54] L.H. Chen, S.M. Lin, Modulation of acetaminophen-induced alteration of antioxidant defense enzymes by antioxidants or glutathione precursors in cultured hepatocytes, Biochem. Arch. 13 (1997) 113–125.
[55] A. Shokouhian, S. Soheili, S. Moradhaseli, L. Fazli, M.S. Ardestani, et al., Toxicity of zinc oxide nanoparticles after repeated oral administration, Am. J. Pharmacol. Toxicol. 8 (2013) 148–154.
[56] R.K. Shukla, V. Sharma, A.K. Pandey, S. Singh, S. Sultana, et al., ROS mediated genotoxicity induced by titanium dioxide nanoparticles in human epidermal cells, Toxicol. In Vitro 25 (2011) 231–241.
[57] M.J. Akhtar, S. Kumar, H.A. Alhadlaq, S.A. Alrokayan, K.M. Abu-Salah, Dose-dependent genotoxicity of copper oxide nanoparticles stimulated by reactive oxygen species in human lung epithelial cells, Toxicol. Ind. Health (2013), http://dx.doi.org/10.1177/0748233713511512.

[58] S. Pakrashi, N. Jain, S. Dalai, J. Jayakumar, P.T. Chandrasekaran, et al., In vivo genotoxicity assessment of titanium dioxide nanoparticles by *Allium cepa* root tip assay at high exposure concentrations, PLOS ONE 9 (2014) e87789, http://dx.doi.org/10.1371/journal.pone.0087789.
[59] E. Demir, N. Kaya, B. Kaya, Genotoxic effects of zinc oxide and titanium dioxide nanoparticles on root meristem cells of *Allium cepa* by comet assay, Turk. J. Biol. 38 (2014) 31–39.
[60] J. Musarrat, Q.S.A. Saquib, A.H. Naqvi Azam, Zinc oxide nanoparticles-induced DNA damage in human lymphocytes, Int. J. Nanoparticles 2 (2009) 402–415.
[61] I.V. Lushchak, Environmentally induced oxidative stress in aquatic animals, Aquat. Toxicol. 101 (2011) 13–30.